Aerodynamic Shape Optimization of a Hypersonic Inlet Configuration

Shlomy Shitrit[1]
RAFAEL, *Advanced* Defense Systems, Ltd., Haifa 31021, Israel

The most suited air breathing vehicle to hypersonic flight is the supersonic combustion ramjet, or scramjet. One of the many challenges to scramjets is being able to operate efficiently over a wide range of flight conditions. Under the extreme pressure and heat experienced at these flight conditions there is a high degree of shape uncertainty. Numerous phenomena such as inlet unstart, extreme load, boundary-layer effects and shear layer interaction, restrict scramjet design and limit their performance. Such problems are the main motivation for surface sensitivities that can be used for aerodynamic shape optimization. The objective of the present paper is to document lessons learned from aerodynamic shape optimization of the HiFire scramjet configuration under supersonic flow conditions. Mesh warping and geometry parametrization is accomplished by using surface control points embedded with free-form deformation (FFD) volumes. The aerodynamic model solves the RANS equations with Spallart-Almaras turbulence model. A gradient based optimization algorithm is used with an adjoint method in order to compute the objectives and constraints derivatives with respect to the design variables. The main purpose of this study is to suggest an approach for aerodynamic shape optimization of scramjet inlet and mainly to present two optimization problem formulations which includes different objectives: pressure recovery and thrust, by using a polynomial approach which reflects a low fidelity model of the combustion and expansion process. The results of optimization are presented, including the tradeoff between the two approaches.

Nomenclature

C_d	=	drag coefficient
C_l	=	lift coefficient
C_p	=	Pressure coefficient
baseline	=	initial configuration
c	=	chord length, m
CRM	=	common research model
ADODG	=	aerodynamic design optimization discussion group
E	=	energy, J
FFD	=	free form deformation
GCI	=	grid convergence index
L	=	grid level
M	=	Mach number
N	=	number of design variables
p	=	static pressure, Pa; order of convergence
R	=	residual
ref	=	reference value
Rey	=	Reynolds number
S	=	area, m^2
t	=	thickness, m
T	=	thrust

[1] Research Engineer, CFD group, Aeronautical Systems, P.O. Box 2250; shlomy.shitrit@gmail.com

PR	=	pressure recovery
u, v, w	=	velocity components, m/s
V	=	volume, m^3
$y+$	=	yplus
α	=	angle of attack, deg
ρ	=	density, kg/m^3

I. Introduction

Scramjet and ramjets offer an attractive means of powered hypersonic flight due to their high specific impulse compared with conventional rockets. Scramjet is an air breathing vehicle that compresses (with no mechanical or moving parts) the air over the inlet, in order to achieve the necessary conditions for supersonic combustion. These hypersonic configurations operate in Mach range of 5 to 10 at the current level of technology. One of the many challenges to scramjets is being able to operate efficiently over a wide range of flight conditions. A scramjet cannot accelerate a vehicle from rest since the inlet compression conditions and temperature are not suitable for combustion. Additionally, at high altitudes the air density becomes so small that the thrust vanishes [1]. There are numerous phenomena that restrict scramjet design and limit performance. Some of them include thermal choking, inlet unstart, extreme heating loads, and boundary layer effects. Under the extreme pressure and heat experienced at these flight conditions there is a high degree of shape uncertainty. The risk of inlet unstarts, the requirement to operate at a wide range of conditions (access to space) and shape uncertainty is the main motivation for surface sensitivities that can be used for aerodynamic shape optimization.

Shape optimization, even only for a wing design, more than ten years ago was a very difficult task. A typical aerodynamic optimization process requires a robust mesh warping method, geometry parametrization, CFD solver and an optimization algorithm. The tremendous improvements in each of these fields in the last few years, and the fact that research groups made them available as an open source tools, allow aerodynamicists in academy as well as in industry to actually perform an aerodynamic shape optimization, and robustly explore a design space that perfectly fits the engineering requirements. These useful tools allow not only for improving existing designs, but also to reach unconventional configurations with much improved performance [2]. Numerical optimization approaches are usually categorized to gradient-based method and gradient-free methods. The adjoint method for computing the gradients along with a gradient-based is proven to be the most efficient method for large scale problems with hundreds of design variables [3] [4] [5] [6]. Pironneau [6] first introduced the adjoint method for drag minimization problems, and then Jameson [7] extended to an aerodynamic optimization of the Euler flow in the late 1980's. Since then various researchers have applied this method within complex implementations for aerodynamic problems [8] [9] [10] [11] [12] [13].

Since the ADODG initiative many publications regarding benchmark problems are available and among the research studies, the multidisciplinary design optimization (MDO) tools are the most remarkable. The research group at University of Michigan is involved in a variety of applications, including the optimization of a supercritical airfoil and starting from a circle [14], aircraft aerodynamics [15] and aero-structural optimization [16], and aero-propulsive optimization. Recently Zhoujie et al. [17] solved a series of aerodynamic shape optimization problems based on the CRM wing. The aerodynamic model solves RANS equations with Spallart-Allmaras turbulence model. A gradient based optimization algorithm is used in conjunction with adjoint method. The drag coefficient is minimized by 8.5% with respect to lift and pitch moment constraints while using 720 shape variables. Other issues such as multi-point optimization, no thickness reduction and starting from random geometry are presented and discussed.

Scramjet engines have been the focus of numerous studies, however an aerodynamic shape optimization which involves the objective definition (thrust and pressure recovery) and the useful restrictions, has received less attention. Recently a great contribution has been published by H. Kline et al. [18] by applying a generalized boundary condition for the continuous adjoint which allows optimization of scramjet engines by facilitating multi-objective approach. The framework they presented allowed to optimize for a balance of thrust and nozzle exit area using low fidelity models of the combustion and expansion process downstream of the inlet. An optimization of a simple two-dimensional scramjet was reported by Matthew Brown et al. [19]. Their optimization algorithm seeks a set of solutions with maximum pressure recovery characterized with a minimum variance. An analytic flow solver is used to solve the inviscid flow within the inlet, and viscous effects and entropy layers were included by using an external CFD package. In 2019, an optimization code, Dakota, was integrated with CFD to optimize a set of parameters for maximum thrust [20]. In this study the fuel injection and combustion were replaced by heat sources. A simplified axisymmetric model was used to find the heat addition for maximum thrust, while applying a genetic algorithm.

Results derivative-based design optimization of turbulent subsonic diffusers was presented by Madsen et al. [21]. They considered the two mentioned approaches shaping the diffuser wall and using guide vanes. A marginal improvement was obtained for diffusers with small area ratio, and the pressure recovery of wide-angled diffusers substantially improved. Madsen et al. [22] also used the response function method to optimize a 2D diffuser. Their goal was to improve the pressure recovery by using two different wall profiles. A small gain in Cp values was obtained (around 1% only). A variation formulation was derived by Cabuk and Modi [23] to determine the diffuser wall profile (with constant width and length) in order to get the maximum static pressure, rise. Their method was applied on a 2D laminar diffuser for maximizing Cp. The performance of the optimized configuration improved dramatically compared to straight line diffuser with the same area ratio at several Reynolds numbers. Wall shaping of a 2D diffuser for maximum Cp was studied by Lund et al. [24]. They used B-spline method to control the wall shape by using 5 control points moving vertically. Only a small improvement of Cp was obtained. Dehghani et al. [25] studied the optimization of laminar flow diffusers by wall contouring with a given length ratio. The developed algorithm uses the commercial CFD software Fluent for the hydrodynamic analysis and employs surrogate modeling for the optimization process. The non-uniform rational basin splines (NURBES) are used to represent the diffuser's wall with three to nine design variables. The CFD analysis and the surrogate model have been combined for a fully automated operation using Matlab. The optimal design exhibits a reasonable performance improvement compared with the reference design.

The present paper demonstrates a modest experience and first steps done towards the construction of an aerodynamic shape optimization capability while applying the ADflow algorithm which is part of the MDO lab framework [26] that was made available as an open-source (2019-2020). The over aim of this article is to improve the performance of the HiFire (Hypersonic International Flight Research Experimentation) scramjet inlet in terms of pressure recovery and uninstalled thrust as objectives. HiFire is a cooperative flight test program between the united states and Australia [27] [28]. One of the main program goals is to gather basic research data on aspects of hypersonic flight not easily accessible to ground testing. In the present study HiFire inlet configuration was chosen as a benchmark problem for CFD validation since its geometry is publicly available [29], including experimental and numerical results in various flow conditions. It is important to mention that the present study is followed by an intensive validation study performed by solving the ADODG (AIAA Aerodynamic Design optimization Discussion Group) benchmark cases, a great initiative that allow researchers around the world to run, compare and make a special thorough analysis of getting the best optimal shapes [17] [30].

The tools that are used for this study are a subset of the multidisciplinary design optimization (MDO) framework of aerodynamic configurations (MACH) [31]. With this software one can perform aero-structural optimization, but in the present study only the MACH's components relevant for aerodynamic shape optimization are used: the CFD solver, mesh warping, geometric parametrization and optimization

algorithm. The remainder of this paper is outlined as follows: The introduction of the optimization tools is briefly described in Section 2. Sections 3 and 4 describe the shape optimization results of the HiFire inlet for pressure recovery and thrust as objectives. Section 5 outlines conclusions.

II. Methodology

The drag minimization of the problems presented in this work is obtained by using a CFD solver coupled with an adjoint solver to compute the objectives and constraints sensitivities, a robust mesh warping routine and a gradient based optimizer. These tools are part of the MACH framework which has been proven to be a useful tool for aero-structural optimization [26]. The pyGeo routine was used for geometric manipulation, iDWarp for mesh deformation, ADflow as the flow solver and SLSQP as the numerical optimization algorithm [26].

A. CFD solver

The CFD solver used in this research is three-dimensional multi-block structured finite volume solver (ADflow). This parallel implicit solver is capable of solving the Euler and Reynolds averaged Navier-Stokes (RANS) equations (steady and unsteady) [32]. The discretization of the governing equations is done by a finite volume approach with a central formulation over structured meshes. The convective terms are computed by the Jameson-Schmidt-Turkel [33] scheme using flux splitting upwind scheme with Van-Albeda limiter. Viscous fluxes are computed to second order accuracy using a central difference approach. The residual smoothing is made by employing an explicit 5th order Runge-Kutta algorithm employing well known steady-state acceleration techniques including local time stepping, and geometric multigrid. For RANS analysis the turbulent equations are solved in coupled fashion using diagonally-dominant alternating direction implicit (DD-ADI) scheme. In order to improve convergence, the solver is also equipped with a diagonallized ADI method for the mean flow equations and Newton-Krylov (NK) solver. The computational coordinates are x, y and z axes, while x in the stream-wise direction, y vertical, and z span-wise. The origin is located at the tip of the nose.

B. Free Form Deformation (FFD) and mesh warping

The geometry parametrization is done by the FFD approach [34]. In this approach the geometry is located inside a B-Spline control volume while the coordinates are mapped to the external surface of the volume by a Newton search algorithm. All the geometric modifications are made on the external surfaces of the FFD volume. Any modification of the FFD boundaries indirectly modifies the internal geometry. The main assumption of this approach is a constant topology throughout the optimization process. The mesh is warped in order to solve the flow field for the modified configuration. In this work the algebraic mesh perturbation scheme is used, which is developed by Kenway et al. [34].

C. Optimization algorithm

In this research work the SLSQP optimization algorithm is applied. It is part of the pyOptSparse framework Perez [35] which is an open source software. SLSQP is a sequential least square programming algorithm [36] that evolved from the least squares' solver [10]. It uses a quasi-Newton Hessian approximation and an L1-test function in the line search algorithm.

III. HiFire inlet aerodynamic shape optimization

A. Background

Two key parameters describe the performance a scramjet inlet: how much compression is performed, and what level of flow losses does the inlet generate during the compression process [Smart]. A schematic view of the internal flowpath of a scramjet is shown in Figure 1. Station 0 is in the free stream flow ahead of the inlet, station 1 is downstream of the inlet forebody shock. Station 2 is at the inlet throat, which is usually the minimum area of the flowpath. The region between stations 2 and 3 is referred to as the

isolator. Station 3 is the combustor entrance, where fuel and air are mixed and burned by the end of the combustor, at station 4. The flow is expanded in the nozzle, between stations 4 and 9, and an external expansion to station 10, at the end of the vehicle. In the present paper the computational model includes the inlet section only, namely stations 0-2.

As already mentioned, several quantities of interest could be used for optimization, and the objective function that is used in the present study directly determines the outcome. For inlet optimization, the inlet total pressure ratio is often maximized, and it is defined as, $PR = P2/P0$, where P2 and P0 are the averaged outlet and inlet total pressures. The main advantage of using the PR as a key parameter for the inlet performance is that it gives an accurate information regarding the inlet compression level. Too much compression can place unnecessary system constraints on the inlet geometry (i.e. variable geometry to start the inlet) and also flow bleed can lead to significant losses and high external drag. To little compression may damage the combustion process and even to start difficulties.

Other options related to the inlet performance is the inlet kinetic energy efficiency, $\mu ke = \frac{v_2'}{v_0} = \frac{h_{t2} - h_2'}{h_{t0} - h_0}$. The usefulness of this parameter is that it can be used for real gas processes, and that its value has been found to be relatively independent of flight Mach number for a particular class of inlets (Smart). The thrust is not directly used as an objective function due to the complexity of evaluating the function. In the present work, similar to work presented by Kline et. al [18], that complexity is managed through the use of low fidelity model combustion and expansion processes downstream of the isolator. A polynomial-based thrust model is used by transferring the averaged outlet mass-flow rate, total pressure and Mach number values as inputs in the thrust equation. The adjoint-based aerodynamic optimization process "treats" the downstream model as a "black box".

The polynomial uninstalled thrust model (see Eq. 1) is constructed by calculating the properties of the flow as it passes through the combustion chamber and the expansion components. At station 3 of the engine's flowpath, the air enters the combustion chamber, where fuel is mixed with air. A constant pressure combustion is assumed, namely, that the exit static pressure of the combustion chamber and the entrance static pressure are equaled, $p_3 = p_4$. The outflow freestream values were obtained by assuming adiabatic expansion.

$$T_x = c_1 + c_2 p + c_3 \dot{m}_{out} c_4 (\dot{m}_{out})^2 + c_5 \dot{m}_{out} \emptyset + c_6 M_{out} \dot{m}_{out} + c_7 \dot{m}_{out} p_t + c_8 \emptyset^2 \dot{m}_{out} \quad (1)$$

Where M is the Mach number, Ps is the static pressure, Pt s the outlet total pressure, $\emptyset = 0.7$ is the fuel-air mass flow fraction, A is the outlet cross-sectional area, and $\dot{m}$ is the mass flow rate. The constant coefficients are given in Table 1.

Table 1: Poynomial coefficient of the thrust model

c_1	c_2	c_3	c_4	c_5	c_6	c_7	c_8
-96.92	$4.42e^{-5}$	587.6	-9.1	-880	-128	$3.96e^{-5}$	1089

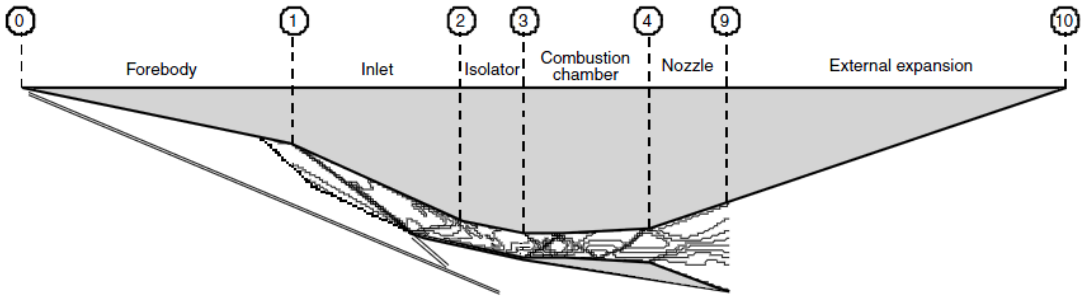

Figure 1:Flow stations in scramjet engine (picture taken from Smart [37])

A. Baseline geometry and flow conditions

Figure 2 shows a side view of the scramjet inlet geometry, not including the combustor and nozzle stages. The overall length is 2250mm, with a constant width of 230 mm. The isolator has a constant length of 370 mm, whereas the top and bottom walls (body and cowl sides) of the inlet diverge at a constant angle of 2.6 deg. The nominal flight condition is a cruise Mach number of $M = 6.0$ in 26 km height. The boundary conditions are supersonic inflow and outflow, no-slip isothermal surfaces on the inlet internal and external walls, and symmetry along the inlet axis.

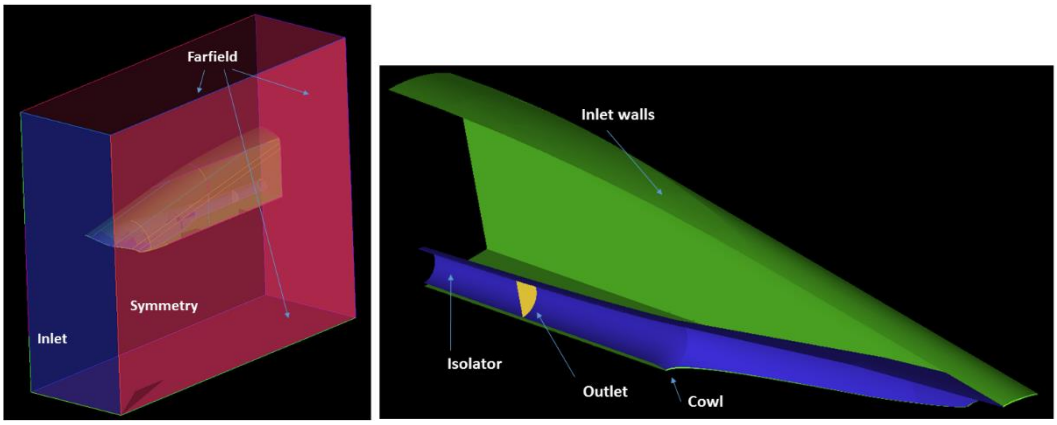

Figure 2: Schematic representation of the HiFire computational model and boundary conditions, not including the combustor and nozzle stages.

B. Grid convergence study

A grid convergence study has been conducted based on the Grid Convergence Index (GCI) method, for examining the spatial convergence of CFD simulations presented in the book by Roache [38]. Roache suggests a GCI can be used to provide a consistent manner in reporting the results of grid convergence studies and also an error band on the grid convergence of the solution. This approach is also based upon a grid refinement estimator derived from the theory of Richardson Extrapolation [9]. The GCI for the fine grid is defined as: $GCI_{fine} = \frac{F_s}{r^p - 1}$ where F_s is a factor of safety (recommended to be $F_s = 1.25$ for comparisons over three or more grids). The GCI for the coarser grid is defined as $GCI_{fine} = \frac{F_s r^p}{r^p - 1}$, while each grid level yield solutions that are in the asymptotic range of convergence for the computed solution. The parameter p is the order of convergence (here a second order accuracy is involved, so theoretically the maximum value is p=2), and r is the effective grid ratio: $r = \left(\frac{N_1}{N_2}\right)^{1/d}$ where N is the total number of

grid points in executive grid levels, and d is the flow dimension. The asymptotic range of convergence can be checked by observing the two GCI values as computed over three grids, $GCI_{23} = r^p GCI_{12}$, while values approximately unity indicates that the solution are within the asymptotic range of convergence.

A structured multi-block mesh with a total number of 30 blocks is constructed by using ANSYS ICEM-CFD commercial software. The mesh convergence study is performed by three levels of grid refinement in order to assess the effect on the numerical accuracy, while the results of each grid level are summarized in Table 2. The grids (see

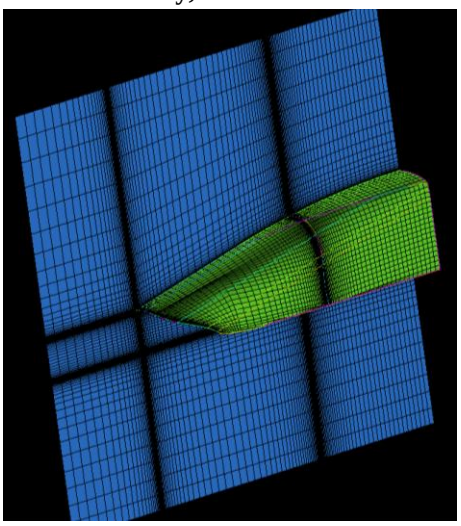

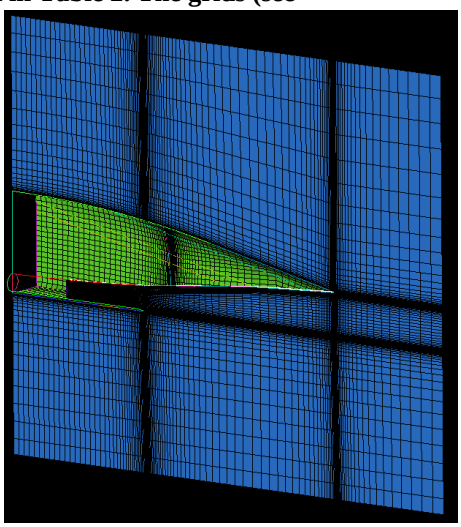

Figure 3) were generated with clustering cells near the walls which results in a range of $y^+ \approx 1-6$. In this grid convergence study, an integer 2 grid coarsening is used, although halving the grid may put the solution out of the asymptotic range. The same grid generation parameters were maintained as the original coarse grid.

The GCI values including the asymptotic range of convergence and an estimation of the aerodynamic coefficient values at zero grid spacing are detailed in Table 2, computed at $\alpha = 0^{\circ}$. Based on this study one can say that, PR is estimated to be 0.522 with an error band of 3.05%. The grid resolution studies confirmed that the computed average outlet mass flow, $mdot$, is grid converged (Table 2).

It is clearly seen that fine mesh analysis shows that there is some benefit to make an optimization on a finer mesh. However, since all this aerodynamic optimization study is done for an industrial application, the subsequent single-point problems are conducted using the coarse mesh (Level L1). In this mesh level the error band in predicted PR value is 5%. Since the optimized configuration is obtained with a very gentle walls movements, (in contradiction to wing shape optimization, where large deformations are involved in the optimization process towards the optimized configuration). The coarse meshes (L1, L2)

do not resolve the flow as accurately, but they still provide derivatives that point the optimizer in the direction of the true optimum.

Table 2: Results of the mesh convergence study for the HiFire scramjet configuration

Mesh level	Mesh size	Mesh ratio, r	GCI [%]	PR	Outlet mass flow [kg/s]	Outlet average Mach number	Y+
L00	∞	-	-	0.522	-	-	-
L0	1867776	1.0	-	0.510	-4.216	2.633	0.1
L1	233471	2.0	3.05	0.484	-4.196	2.624	1.6
L2	29184	4.0	10.03	0.402	-3.994	2.452	8.1

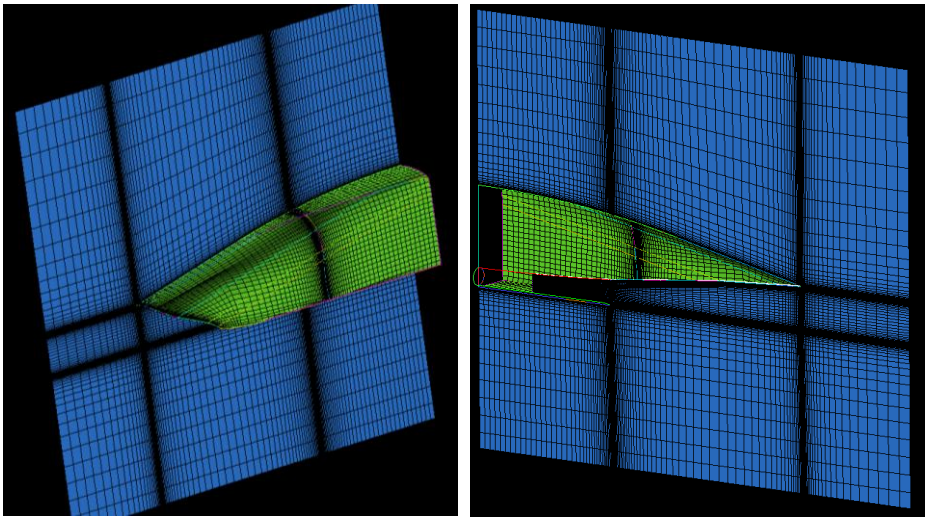

Figure 3: Structured mesh (Level L1) generated by using ICEM-CFD commercial software

C. Optimization problem formulation

Two practical objectives, pressure recovery and thrust, are considered in the design of an optimized scramjet inlet. The level of compression performed by a scramjet inlet can have a significant influence on the overall efficiency of the engine. In addition, there are numerous practical constraints on the compression level [37] of a scramjet that must be considered during the design process. The most important of these were suggested by Smart [37]: 1. non-equilibrium flow effects in the nozzle, 2. operability limits related to inlet starting and boundary-layer separation, and 3. robust combustion requirements. Constraints 1 and 2 put a practical constraint on the maximum allowable compression level, whereas constraint 3 put a practical constraint on the minimum allowable compression level. In the present study an upper limit throat Mach number were chosen as the constraint for increasing the pressure recovery (the first case) and the uninstalled thrust (the second case). This constraint is chosen from both, robust combustion requirements (constraint 3) and boundary layer separation (constraint 2) point of view. The motivation of limiting the throat Mach number affects the scramjet design in three

ways: First, because of the high velocity of the airflow through a scramjet, the combustion process must be rapid in order to be completed before the air exits the engine. On the other hand, the drag and heat load of the combustor have been found to be important parameters for overall scramjet system design, therefore combustors should be as short as possible [37].

Second, restricting the outlet Mach number (at the end of the isolator – the combustor entrance) may cause an increased pressure and also increases the temperature. This is advantageous, as higher temperatures will improve the cycle efficiency of the engine, and additionally, in conjunction with the higher pressures, will reduce the ignition and reaction times. Ignition and reaction times are of critical importance to scramjets due to high velocity of the internal flow through the engine. High velocities result in a very short residence time of the flow in the engine.

Third, the flow through a hypersonic inlet will be turbulent and can be prone to boundary-layer separation due to shock interactions. Large-scale boundary layer separation (which can be a result of both high Mach number and long inlets) can create blockage of the engine and unstart. In practice, it is the desire to reduce boundary-layer separation by setting a limit on the flow velocity through the isolator. In both cases, pressure recovery and thrust are maximized subject to a maximum outlet Mach number $M_{outlet} \leq 2.2$.

Table 3: Design variables

Design variables	Count	Type
inlet shape	168	Y,Z direction

Table 4: Constraints

Constraints	Count	Type
Outlet Mach number	-	≤ 2.2

Table 5: Cases calculated in this research work

Case	Design variables	Objective	Constraints	Mesh level
1	inlet shape	PR	Outlet Mach number	**L1**
2	inlet shape	Thrust	Outlet Mach number	**L1**

D. The FFD parametrization

The inlet geometry is parametrized using two FFD volumes. The internal walls of the inlet, from the nose to the outlet surface are enveloped within 2 FFD blocks, while the cowl tip is the interface between FFD-1 and FFD-2. The design variables (listed in

Table 3) are the y and z coordinates of the 168 control points, distributed uniformly. In order to control the upper wall shape, the coordinates of each control point are constrained by the upper and lower bounds (see

Design variables	Count	Type
inlet shape	168	Y,Z direction

Table 4: Constraints

Constraints	Count	Type
Outlet Mach number	-	≤ 2.2

Table 5: Cases calculated in this research work

). The bounds values are FFD-mesh dependent, and are predefined according to the interval between the FFD-2 control points. The lower and upper bounds for the different cases are summarized in

Design variables	Count	Type
inlet shape	168	Y,Z direction

Table 4: Constraints

Constraints	Count	Type
Outlet Mach number	-	≤ 2.2

Table 5: Cases calculated in this research work

.

In order to increase the flexibility of the optimization problem, the outlet section is not fixed in space. The upper and lower walls of the outlet section (FFD-2) are allowed to move as a solid body in the y-direction only, and the side wall is allowed to move in z-direction only. The control points (FFD's 1-2) along the symmetry plane are defined to move in y-direction (symmetry plane). All the others control points are allowed to move in both y and z directions. The coarse FFD has three control points in the z-direction and 14 control points distributed evenly in the stream wise direction, making a total of 168 FFD points (for half configuration). Table 6 lists the optimized pressure recovery values four cases the number of design variables (as also shown in Figure 5-Figure 7), and shows that doubling the number of design variables from 84 points to 168 control points, the pressure recovery values decrease. Although increasing the number of design variables improves the geometry representation, it also caused much more difficulties for the flow solver because of high frequency shape variations. This issue caused the optimization using 252 design variables for the inlet case to fail. I tried different numbers of design variables distribution, but only the more interesting results are shown here. The flow converges to a density residual of 10^{-5} and the adjoint equation convergence was set to 10^{-8}. The optimality convergence tolerance of SLSQP optimization algorithm was set to 10^{-6}. The initial design point for all the optimizations is the baseline geometry, unless stated otherwise. The optimizations are performed using an eight-core 3.5GHz Intel processors pc with 32GB RAM.

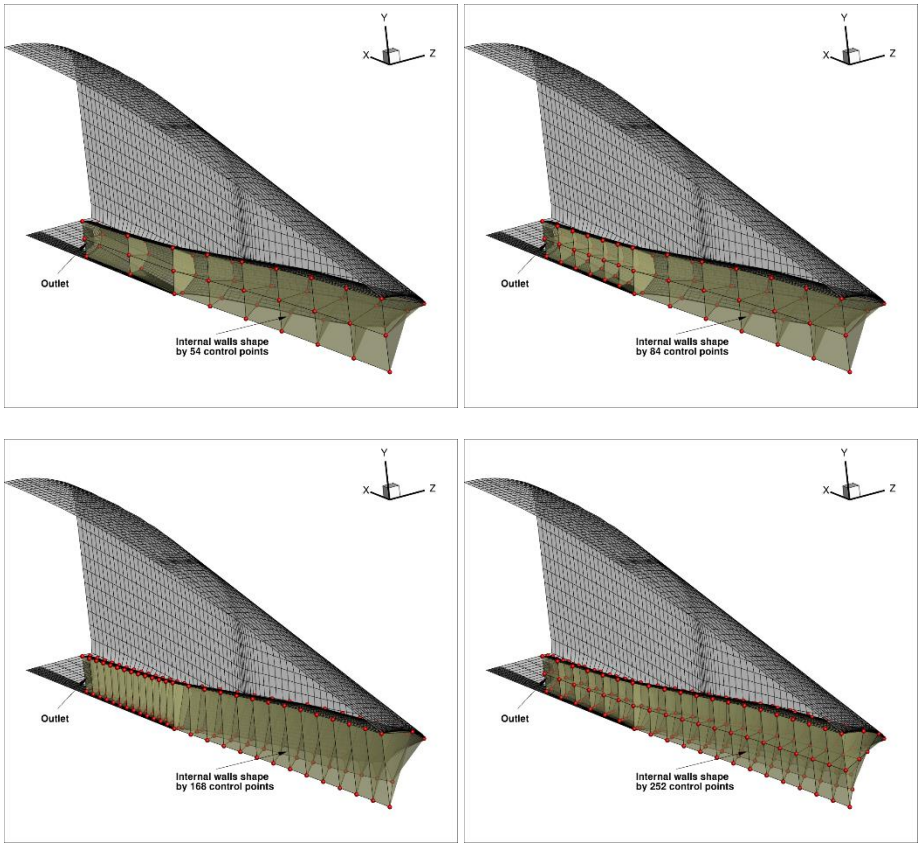

Figure 4: Example of FFD volumes with 54, 84, 168 and 252 control points (red points).

Table 6: Pressure recovery values as a function of the number of design variables.

Number of design variables, N	Pressure recovery, PR
54	0.512
84	0.513
168	0.458
252	Fail

The main purpose of this study is to suggest an approach for aerodynamic shape optimization of scramjet inlet and mainly to present two optimization problem formulations which includes different objectives: pressure recovery and thrust. The results of optimization studies will then be presented, including the tradeoff between the two approaches. It is important to mention here that, in both cases robustness issues with the optimization process were encountered. It took quite some time to define the appropriate parameters values (such as numerical setup, FFD design variables deformation strategy) in order to reach a stable and clear convergence of the desired objectives and constraints. In addition, the geometric parametrization involves a simple FFD which includes only two simple hexahedra volumes, but the geometry of these volumes and the way they "follow" the deformed walls, has a tremendous effect on the overall robustness of the optimization process. By "robustness" the author means the capability of the aerodynamic optimization process to converge to the actual optimal shape starting from a wide range of flow conditions (or shapes). For a given aerodynamic design problem, a robust setup should be able to parametrize the shape, deform the mesh while maintaining a high mesh quality, and produce a well

converged CFD solution. There were a lot of troubleshooting issues in many aspects of the optimization process which were time consuming, in order to identify the key features needed for getting a robust optimization process.

E. Maximizing the Pressure recovery

In this first study the results of the aerodynamic shape design optimization of the inlet configuration are presented. This problem is single objective and single constraint. The design variables are the 81 shape control points on the inlet internal walls. Only a maximum area-average Mach number constraint is imposed on the outlet surface, therefore, one flow solution and three adjoint solutions (inlet and outlet total pressure, and average outlet Mach number) are needed at each design iteration. The final results are listed in Figure 5. The optimization process is started with the DDADI until a reduction of three orders of magnitude in the total residual norm is achieved. Then the solver is switched to ANK for better performance. The relatively selected lower convergence level ($O(10^{-3})$) for the switch between the solvers improves the robustness of the nonlinear solver (although it comes at the cost of sub-optimal performance for simpler cases). The optimality convergence condition in SLSQP is 10^{-5}.

Convergence is reached within 2.34 hours using 7 processors (for mesh level L1), with 45 calls to the objective function and 14 calls to the sensitivity analysis function. The convergence history of the aerodynamic coefficients (mesh L1) is shown in Figure 5-Figure 7 for three cases of the number of design variables. The optimized inlet has a 5.1% lower pressure recovery value than the baseline configuration. The pressure recovery is decreased from 0.483 to 0.458. This moderate decrease in the inlet efficiency does not tells the whole story. The slightly decreased pressure recovery comes with a lower Mach number at the isolator (2.04 compared to 2.62 for the baseline configuration). The outlet area decreased from 0.00519 to 0.00287 (see Figure 7). A comparison of the optimized and baseline inlet, with the Mach number distribution on the symmetry plane, is presented in Figure 8. The flow process in the throat area towards the isolator, is characterized by a series of complex multiple interactions of shock waves with the turbulent boundary layer, usually referred to as a "normal shock train". On the one hand, it is clearly seen that the shape design variables make a significant contribution to minimize the outlet Mach number and fulfill the constraint. On the other hand, the inlet forebody was slightly deformed. Similar shocks were obtained, while the main geometrical deformations accrued from the cowl and downstream. The initial geometry exhibits higher velocity after the cowl. We would expect the optimizer to seek for weaker shock solutions, but a reduction of the throat area directly affected the pressure. The final step of the optimizer is shown in Figure 9, superimposing the optimized geometry (in yellow) on the baseline geometry (in grey).

This optimization problem is challenging to converge mainly because it is very sensitive to the mesh warping procedure and the control points movement's range. At the first experience the lower and upper bounds of the Y-coordinate control points were defined $\pm 20\ mm$, respectively. This general and straightforward approach results in failures in the warping procedure after few iterations since the vertical deformations in the nose region. Therefore, in order to overcome this limitation, no unified lower and upper thickness bounds are defined, in a way that the inlet is divided to three stream wise sections: nose, cowl and outlet surface.

Since the optimization algorithm reached the lower and upper bounds, during the optimization procedure, mainly in the fore-body (in FFD-1), it is definitely an evidence that the optimization algorithm "would like" to wrap even more, so widening the bounds might improve the optimized pressure recovery obtained. The reason for these bounds definition beforehand is due to multiple mesh failures during warping process. So, a possible approach to improve the scramjet performance even better is to start a second optimization process while using the optimized configuration which obtained at the end of the first optimization cycles as the new baseline configuration. In this way we might probably achieve even more improvement in the inlet performance.

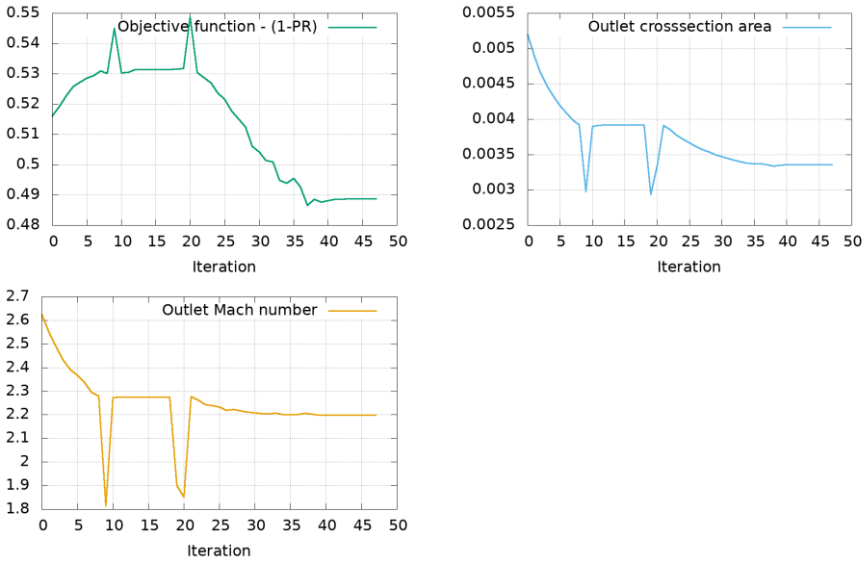

Figure 5: Covergence of the pressure recovery (top left), outlet cross-sectional area (top right) and outlet Mach number (bottom left) as a function of the iterations number, calculated with 54 design variables.

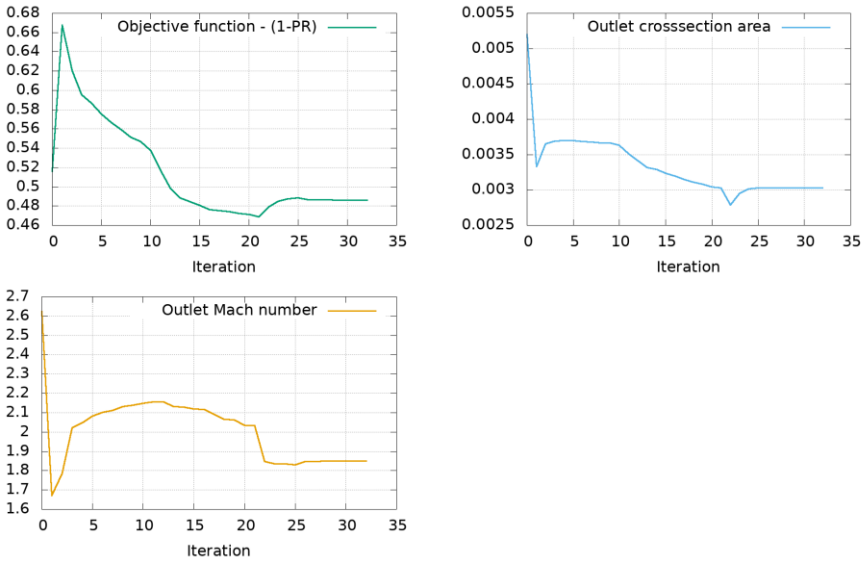

Figure 6: Covergence of the pressure recovery (top left), outlet cross-sectional area (top right) and outlet Mach number (bottom left) as a function of the iterations number, calculated with 84 design variables.

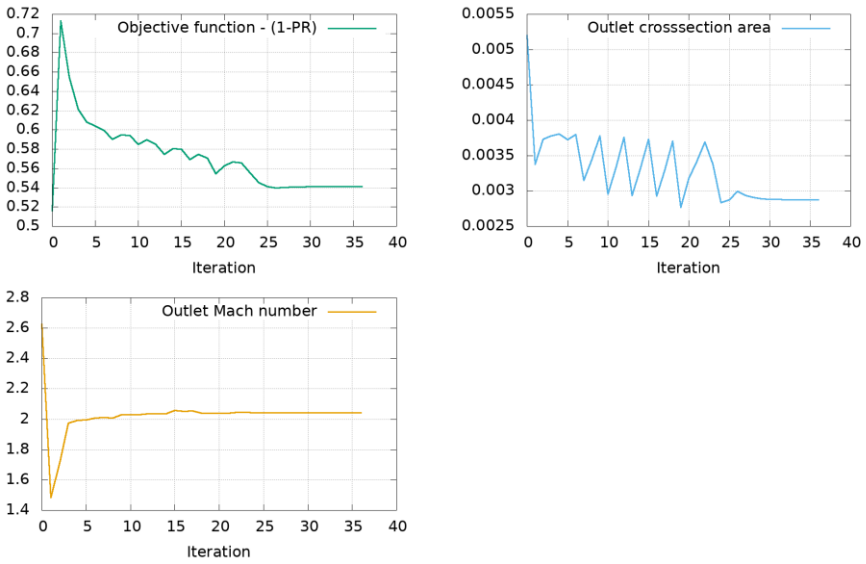

Figure 7: Covergence of the pressure recovery (top left), outlet cross-sectional area (top right) and outlet Mach number (bottom left) as a function of the iterations number, calculated with 168 design variables.

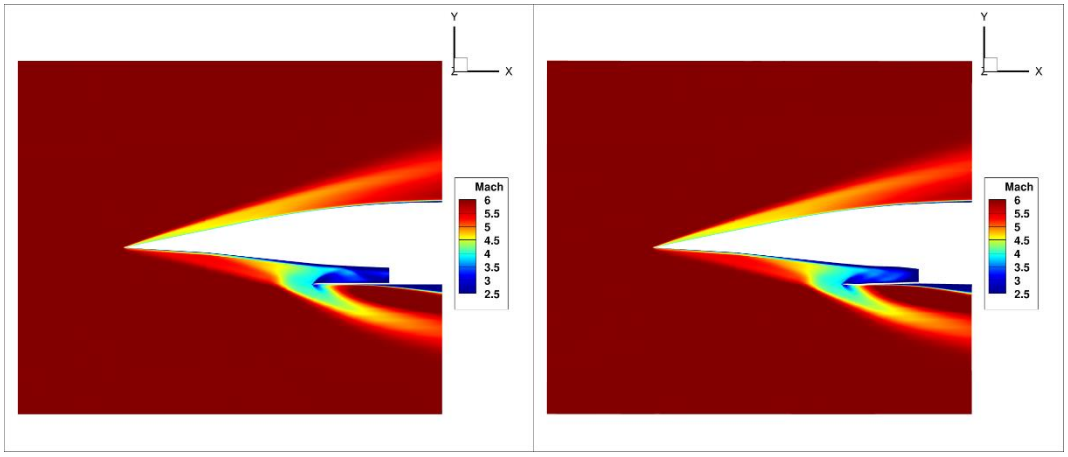

Figure 8: Mach number distribution on the symmetry plane for the baseline design (left figure), and the optimized configuration for maximum pressure recovery (right figure).

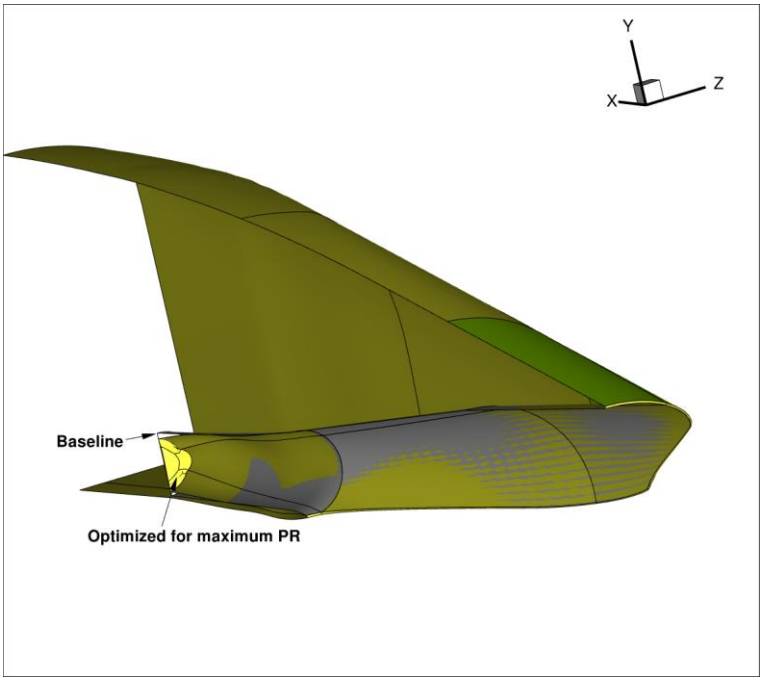

Figure 9: Maximum pressure recovery optimization results, superimposing optimized geometry in yellow on initial geometry in grey.

F. Maximizing the thrust

In this section the same problem is solved but this time, the uninstalled thrust (Eq. 1) is maximized subject to a constraint of maximum Mach number of 2.2 at the throat. The optimization process while using the thrust as the objective is more computationally costly than maximizing the pressure recovery, since few variables such as: outlet total pressure, average Mach number, mass flow rate, must be integrated on the fly, during the optimization process in order to obtain the thrust. Convergence is reached within 2.5 hours using 7 processors (for mesh level L1), with 15 calls to the objective function and 3 calls to the sensitivity analysis function. Due to the large deformation applied mainly from the cowl downstream, the optimization process was not able to converge while using the upper bounds (20mm for FFD-2) defined in the previous case. Therefore, moderate upper bounds of 10 mm for FFD-2 were used for optimization of thrust in the same flow conditions. The convergence history of the thrust and outlet Mach number is given in Figure 10. In order to illustrate the solver seeking for higher thrust, the history data of the outlet area and mass flow rate is also presented.

The thrust is improved by 21.7% compared to the initial design, and it has increased from $557\ N$ $to\ 712\ N$ (for half configuration). Due to the moderate control points upper bounds chosen, the outlet area was slightly increased from $0.00519\ m^2$ to $0.00548\ m^2$. The Mach number constraint is achieved with a wide optimized geometry, mainly from the cowl section and downstream. In contradiction to the maximum pressure recovery optimization problem, the optimizer has specified the compression efficiency in favor of higher thrust. When optimizing the thrust, which includes a low-fidelity polynomial that reflects the combustion and expansion components, the efficiency of the compression (pressure recovery at the throat) is actually decreased. A decrease of 35% on the pressure recovery is correlated with an overall increase of 21% in thrust, when optimizing the thrust.

It is also interesting to note here that a maximum allowable deformation of the internal walls has been produces, between the cowl and the outlet section, were the reflected shock meets the wall. It is assumed that continuing the optimization while starting from the optimized geometry might result in an even better thrust performance. The final step of the optimizer is given in Figure 12 as superimposing the initial

design in grey on the optimized design in yellow. The mass flow rate calculated at the outlet is raised (mainly due to larger outlet area), which directly raises the thrust.

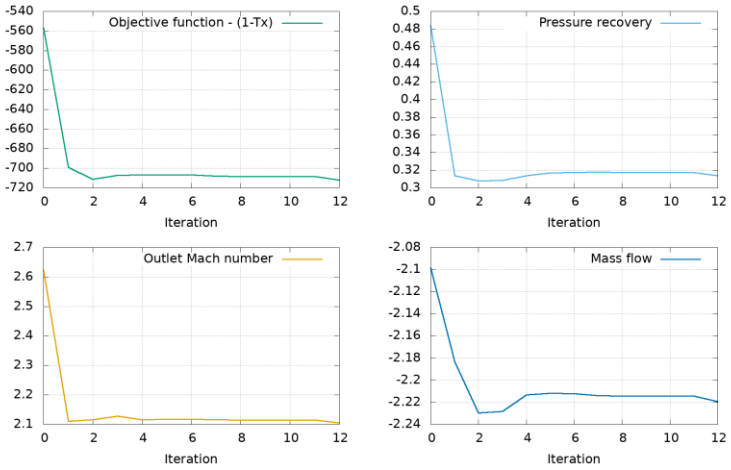

Figure 10: Results obtained for maximum thrust optimization. Covergence of the thrust (top left), pressure recovery (top right), outlet Mach number (bottom left), and outlet mass flow rate (bottom right), as a function of the iterations number.

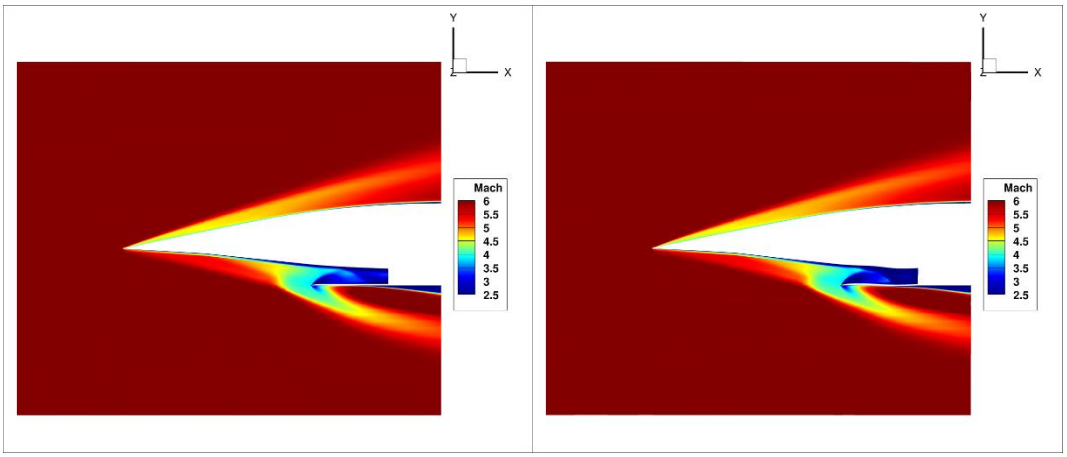

Figure 11: Mach number distribution on the symmetry plane for the baseline design (left figure), and the optimized configuration for maximum thrust (right figure).

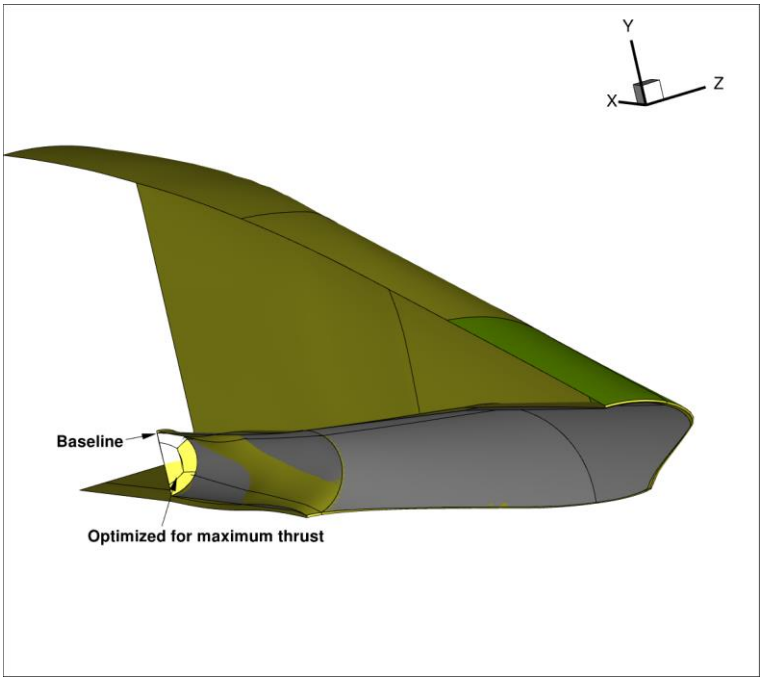

Figure 12: Optimizatin for maximum thrust results, superimposing optimized geometry in yellow on initial geometry in grey.

IV. Conclusions

This paper presents a modest experience to construct an aerodynamic optimization capability based on the gradient based algorithms together with an adjoint method that computes the required gradients efficiently, developed by the University of Michigan MDO Lab. The main motivation for this research is analyzing the sensitivity and robustness of the flow solver, mesh warping method and the optimization algorithm to reduced sized problems, in a way that would fit the time and resources limitations that exists in industrial applications. The effectiveness of the optimization process is demonstrated by benchmarking the HiFire inlet scramjet geometry for two different objectives. For both cases well, converged results were obtained.

The first case includes optimizing the pressure recovery at the inlet throat by constraining the average Mach number at the throat. The optimized inlet has a 5.84% higher pressure recovery than the baseline configuration. The main challenge of this problem involves minimizing the throat area in order to reduce the Mach number and increase the static pressure. Both, initial and optimized design have similar shock formation.

In the second case the optimization is done for thrust subject to a maximum Mach number constraint at the throat. When optimizing the thrust, which includes a low-fidelity polynomial that reflects the combustion and expansion components, the efficiency of the compression (pressure recovery at the throat) is actually decreased. A decrease of 35% on the pressure recovery is correlated with an overall increase of 21% in thrust, when optimizing the thrust.

In this research the robustness of the flow solver and mesh warping algorithm is demonstrated by optimizing a scramjet geometry with respect to pressure recovery and thrust objectives. In spite of the fact that this preferred scramjet geometry might not be of interest for industrial applications, it definitely examines the robustness of the numerical method as well as the FFD parametrization method.

V. References

[1] A. N. Ridings, "Investigation of Pre-Combustion Shock Trains in a Scramjet Using a Shock Tunnel at Mach 8 Flight Conditions," The University of Queensland School of Mechanical and Mining Engineering, 2014.

[2] A. Ning and J. R. R. A. Martines, Engineering Design Optimization, University of Michigan and Brigham Young University, 2021.

[3] J. Peter and R. P. Dwight, "Numerical sensitivity analysis for aerodynamic optimization: A survey of approaches," *Computers and Fluids,* pp. 373-391, 2010.

[4] J. R. R. A. Martins and J. T. Hwang, "Review and unification of methods for computing derivatives of multidisciplinary computational models," *AIAA,* pp. 2582-2599, 2013.

[5] J. R. R. A. Martins, P. Sturdza and J. J. Alonso, "The complex-step derivative approximation," *ACM Transactions on Mathematical Software,* pp. 245-262, 2003.

[6] O. Pironneau, "On optimum design in fluid mechanics," *Journal of Fluid Mechanics,* vol. 64, pp. 97-110, 1974.

[7] A. Jameson, "Aerodynamic design via control theory," *Journal of scientific computing,* vol. 3, pp. 233-260, 1988.

[8] A. Jameson, "Computational algorithms for aerodynamic analysis and design," *Applied Numerical Mathematics,* pp. 383-422, 1993.

[9] D. A. Anderson, J. C. Tannehill and R. H. Pletcher, Computational Fluid Mechanics and Heat Transfer, New York: McGraw-Hill Book Company, 1984.

[10] C. L. Lawson and R. J. Hanson, "Solving Least Squares Problems," *Classics in Applied Mathematics, SIAM,* p. Volume 15, 1987.

[11] E. J. Nielsen and W. K. Anderson, "Aerodynamic design optimization on unstructured meshes using the Navier{Stokes equations,," *AIAA,* pp. 1411-1419, 1999.

[12] S. Z. Chen, G. K. W. K. Lyu and J. R. R. A. Martines, "Aerodynamic shape optimization of the Common Research Model wing-body-tail configuration," *Journal of aircraft 53,* pp. 276-293, 2016.

[13] Y. Yu, Z. Lyu, Z. Xu and J. R. R. A. Martins, "On the influence of optimization algorithm and starting design on wing aerodynamic shape optimization,," *Aerospace Science and Technology 75,* pp. 183-199, 2018.

[14] H. Xiaolong, L. Jichao, A. M. Charles, A. Yildirim and J. R. R. A. Martines, "Robust aerodynamic shape optimization-from a circle to an airfoil," *Aerospace Science and Technology,* pp. 48-61, 2019.

[15] S. Chen, Z. Lyuy, K. W. K. Gaetan and J. R. R. A. Matines, "Aerodynamic Shape Optimization of the Common Research Model Wing-Body-Tail Configuration," in *AIAA SciTech Forum*, Florida, 2015.

[16] J. R. R. A. Martins, "Multidisciplinary Design Optimization of Aircraft Conigurations," Von Karman Institute for Fluid Dynamics, Belgium, 2016.

[17] Z. Lyu, K. W. Gaetan and J. R. R. A. Martins, "Aerodynamic Shape Optimization Investigations of the Common Research Model Wing Benchmark," *AIAA Journal,* 2014.

[18] H. L. Kline, T. D. Economon and a. J. J. Alonso, "Multi-Objective Optimization of a Hypersonic Inlet Using Generalized Outflow Boundary Conditions in the Continuous Adjoint Method," *AIAA,* 2019.

[19] R. N. Mudford, "Robust Design Optimization of Two-Dimensional Scramjet Inlets," in *14th AIAA/AHI Space Planes and Hypersonic Systems and Technologies Conference*, AIAA 2006-8140, 2006.

[20] N. T. McGillivray, "Coupling Computational Fluid Dynamics Analysis and Optimization Techniques for Scramjet Engine Design," Wright State University, 2018.

[21] J. I. Madsen, N. Olhoff and T. J. Condra, "Optimization of Straight, Two-Dimensional Diffusers by Wall Contouring and Guide Vane Insertion," in *World Congress of Structural and Multidisciplinary Optimization*, Buffalo, NY, USA, 1999.

[22] J. I. Madsen, W. Shyy and R. T. Haftka, "Response Surface Techniques for Diffuser Shape Optimization," *AIAA,* vol. 38, pp. 1512-1518, 2000.

[23] H. Çabuk and V. Modi, "Optimum Plane Diffusers in Laminar Flow," *Journal of Fluid Mechanics,* vol. 237, pp. 373-393, 1992.

[24] E. Lund, H. Moller and L. A. Jakobsen, "Shape Design Optimization of Stationary Fluid-Structure Interaction Problems with Large Displacements and Turbulence," in *World Congress on Structural and Multidisciplinary Optimization*, Dalian, China, 2001.

[25] M. Dehghani, H. Ajam and S. Farahat, "Automated Diffuser Shape Optimization based on CFD Simulations and Surrogate Modeling," *Journal of Applied Fluid Mechanics,* vol. 9, pp. 2527-2535, 2016.

[26] "https://github.com/mdolab/MACH-Aero," Uniuversity of Michigan, 2019. [Online].

[27] D. Dolvin, "Hypersonic International Flight Research and Experimentation (HIFiRE) Fundamental Science and Technology Development Strategy," *AIAA,* p. 2581, 2008.

[28] D. D., "Hypersonic International Flight Research and Experimentation Technology Development and Flight Certification Strategy," *AIAA,* p. 7228, 2009.

[29] B. H. Dauby, D. W. Adamczak, J. A. Muse and M. A. Bolender, "HIFiRE 6: Overview and Status Update 2015," in *International Space Planes and Hypersonic Systems and Technologies Conferences*, Glasgow, Scotland, 2015.

[30] C. Lee, "Aerodynamic Shape Optimization of Benchmark Problems Using Jetstream," *American Institute of Aeronautics and Astronautics,* 2018.

[31] J. R. R. A. Martins, G. K. W. Kenway and T. Brooks, "Multidisciplinary Design Optimization of Aircraft Configurations - part2: High fidelity aerostructural optimization," in *Lecture series, Von Karman Institute for Fluid Dynamics*, Sint Genesius Rode, Belgium, 2016.

[32] E. van der Weide, G. Kalitzin, J. Schluter and J. Alonso, "Unsteady Turbomachinery Computations Using Massively Parallel Platforms," in *44th AIAA Aerospace Sciences Metting and Exhibit*, 2006.

[33] A. Jameson, W. Schmidt and E. Turkel, "Numerical Solution of the Euler equations by Finite Volume Methods Using Runge Kutta Stepping Schemes," in *14th AIAA, Fluid and Plasma Dynamics Coneference*, 1981.

[34] G. K. W. Kenway, G. J. Kennedy and J. R. R. A. Martines, "A CAD-free Approach to High Fidelity Aerostructural Optimization," in *13th AIAA/ISSMO Multidisciplinary Analysis Optimization Conference*, Fort Worth, 2010.

[35] N. Wu, G. K. W. Kenway, C. A. Mader, J. Jasa and J. R. R. A. Martines, "pyOptSparse: a Python framework for large-scale constrained nonlinear optimization of sparse systems," *Journal of open source software*, vol. 5, p. 2564, 2020.

[36] D. Kraft, "A software package for sequential quadratic programming," DLR German Aerospace Center, 1988.

[37] M. K. Smart, "How Much Compression Should a Scramjet Inlet Do?," *AIAA JOURNAL*, Vols. 50, No. 3, March 2012.

[38] P. J. Roache, K. Ghia and F. While, "Editorial Policy Statement on the Control of Numerical accuracy," *ASME Journal of Fluids Engineering*, p. 2, 1986.

[39] J. D. M. R. M. a. W. R. Vassberg, "Development of a Common Research Model for Applied CFD Validation Studies," *American Institute of Aeronautics and Astronautics,* 2008.

[40] V. V. W. K. Anderson, "Aerodynamic design optimization on unstructured grids with a continuous adjoint formulation,," *Computers and Fluids*, pp. 443-480, 1999.

[41] A. Jameson, "Aerodynamic design via control theory," *Journal of Scientific computing*, pp. 233-260, 1988.

[42] C. A. Mader, "ADjoint: An Approach for the Rapid Development of Discrete Adjoint Solvers," *AIAA Journal*, vol. 46, 2008.

[43] R. E. Perez, P. W. Jansen and J. R. R. A. Martins, "A Python-based object-oriented framework for nonlinear contrained optimization, Structural and Multidisciplinary Optimization," 2012.

[44] S. Shitrit, "Aerodynamic shape optimization of benchmark problems," *Journal of mathemtical physics - Vixive.org*, p. 26, 2021.

[45] "http://gosculptor.com," [Online].

[46] D. J. Dolvin, "Hypersonic International Flight Research and Experimentation (HIFIRE)," in *15th AIAA International Space Planes and Hypersonic Systems and Technologies Conference*, Dayton, Ohio, 28 April - 1 May 2008.

[47] D. Adamczak, H. Alesi and M. Frost, "HIFiRE-1: Payload Design, Manufacture, Ground Test, and Lessons Learned," in *16th AIAA/DLR/DGLR International Space Planes and Hypersonic Systems and Technologies Conference*, 2009.

[49] P. H. Cook, M. A. McDonald and M. C. P. Firmin, "\Aerofoil RAE 2822 - Pressure Distributions, and Boundary Layer and Wake Measurements," Experimental Data Base for Computer Program Assessment, AGARD Advisory Report, No 138, 1979.

[50] L. Zhoujie, G. K. K. and J. R. R. A. Martines, "Aerodynamic Shape Optimization Investigations of the Common Research Model Wing Benchmark," *AIAA Journal*, 2014.

[51] K. W. Gaetan and J. R. R. A. Martines, "CRM Wing-Body-Tail Optimization at Flight Reynolds Number," Univerisity of Michigan, 2019.

[52] N. P. B. Martins and J. R. R. A. Martines, "Aerostructural Design Exploration of a Wing in Transonic Flow," in *Aerospace*, Michigan, 2020.

[53] N. Secco, G. K. W. Kenway, P. H. C. A. Mader and J. R. R. A. Martines, "Efficient mesh generation and deformation for aerodynamic shape optimization," *AIAA*, vol. 54, pp. 1151-1168, 2021.